University of Reading

Automated determination of auroral breakup during the substorm expansion phase using all sky imager data

Article

Published Version

Murphy, K. R., Miles, D. M., Watt, C. E.J., Rae, I. J., Mann, I. R. and Frey, H. U. (2014) Automated determination of auroral breakup during the substorm expansion phase using all sky imager data. Journal of Geophysical Research: Space Physics, 119 (2). pp. 1414-1427. ISSN 2169-9402 doi: 10.1002/2013JA018773 Available at https://centaur.reading.ac.uk/36177/

It is advisable to refer to the publisher's version if you intend to cite from the work. See Guidance on citing.

To link to this article DOI: http://dx.doi.org/10.1002/2013JA018773

Publisher: American Geophysical Union

All outputs in CentAUR are protected by Intellectual Property Rights law, including copyright law. Copyright and IPR is retained by the creators or other copyright holders. Terms and conditions for use of this material are defined in the End User Agreement.

www.reading.ac.uk/centaur

University of Reading

CentAUR

Central Archive at the University of Reading

Reading's research outputs online

AGU PUBLICATIONS

JGR

Journal of Geophysical Research: Space Physics

TECHNIQUE

10.1002/2013JA018773

Key Points:
- Automated and quantitative determination of auroral breakup
- Basis for quantitative statistical study of substorms and substorm breakup
- Parameterized algorithm allows specific auroral phenomenology to be targeted

Supporting Information:
- Readme
- Movie S1
- Movie S2
- Movie S3
- Movie S4
- Movie S5
- Movie S6
- Movie S7

Correspondence to:
K. R. Murphy,
kmurphy@ualberta.ca

Citation:
Murphy, K. R., D. M. Miles, C. E. J. Watt, I. J. Rae, I. R. Mann, and H. U. Frey (2014), Automated determination of auroral breakup during the substorm expansion phase using all-sky imager data, *J. Geophys. Res. Space Physics*, *119*, 1414–1427, doi:10.1002/2013JA018773.

Received 26 FEB 2013
Accepted 13 JAN 2014
Accepted article online 20 JAN 2014
Published online 22 FEB 2014

Automated determination of auroral breakup during the substorm expansion phase using all-sky imager data

Kyle R. Murphy[1], David M. Miles[1], Clare E. J. Watt[1,2], I. Jonathan Rae[1,3], Ian R. Mann[1], and Harald U. Frey[4]

[1]Department of Physics, University of Alberta, Edmonton, Alberta, Canada, [2]Now at Department of Meteorology, University of Reading, Reading, UK, [3]Now at Mullard Space Science Laboratory, University College London, Dorking, UK, [4]Space Sciences Laboratory, University of California, Berkeley, California, USA

Abstract This paper describes a novel method for quantitatively and routinely identifying auroral breakup following substorm onset using the Time History of Events and Macroscale Interactions during Substorms all-sky imagers. Substorm onset is characterized by a brightening of the aurora that is followed by auroral poleward expansion and auroral breakup. This breakup can be identified by a sharp increase in the auroral intensity $i(t)$ and the time derivative of auroral intensity $i(t)$. Utilizing both $i(t)$ and $i'(t)$, we have developed an algorithm for identifying the time interval and spatial location of auroral breakup during the substorm expansion phase based solely on quantifiable characteristics of the optical auroral emissions. We compare the time interval determined by the algorithm to independently identified auroral onset times from three previously published studies. In each case the time interval determined by the algorithm is within error of the onset independently identified by the prior studies. We further show the utility of the algorithm by comparing the breakup intervals determined using the automated algorithm to an independent list of substorm onset times. We demonstrate that 50% of the breakup intervals characterized by the algorithm are within the uncertainty of the times identified in the list. The quantitative description and routine identification of an interval of auroral brightening during the substorm expansion phase provides a foundation for unbiased statistical analysis of the aurora and to probe the physics of the auroral substorm and identify the processes leading to auroral substorm onset.

1. Introduction

Magnetospheric substorms are characterized by an explosive release of energy accumulated in the nightside magnetosphere as a result of coupling between the interplanetary magnetic field and the Earth's magnetosphere. Magnetic reconnection on the dayside extracts energy from the solar wind, which is stored in the Earth's nightside magnetosphere in the form of stretched magnetic fields. The accumulation of energy in the nightside magnetosphere is referred to as the substorm growth phase [*McPherron*, 1970]. As more and more energy is stored in the nightside magnetosphere, the magnetic field in the tail becomes increasingly compressed until a critical point is reached and the energy stored in the tail is explosively released during the substorm expansion phase [*Aubry and McPherron*, 1971]. Despite the clear overall path of energy transfer in the substorm process, the details of the physical processes and their time sequence during magnetospheric and ionospheric substorm onset remain highly controversial [e.g., *Angelopoulos et al.*, 2008, 2009; *Lui*, 2009].

During the substorm expansion phase, the cross-tail current is disrupted, the nightside magnetosphere depolarizes, magnetic reconnection in the tail is initiated or further enhanced, and the aurora expands, initially in a localized region and subsequently azimuthally and poleward. In the ionosphere, the sequence of events during the substorm expansion phase onset is very well defined: the most equatorward arc brightens (or a new arc forms equatorward of the growth phase arc) and begins to expand poleward and then ultimately explosively expands across the nightside [*Akasofu*, 1977].

The expansion phase controversy relates to whether current disruption via a localized plasma instability [*Lui*, 1996] in the near-Earth magnetosphere (~10 R_E) precedes magnetic reconnection further down tail (~25 R_E) and is responsible for initiating the substorm expansion phase or vice versa [*Baker et al.*, 1996].

©2014. American Geophysical Union. All Rights Reserved.

Recent work utilizing the Time History of Events and Macroscale Interactions during Substorms (THEMIS) mission [*Angelopoulos*, 2008] has shown strong evidence for both reconnection [*Angelopoulos et al*., 2008] and the potential action of a near-Earth instability [*Rae et al*., 2009a] in triggering substorm expansion phase onset. Another substorm paradigm suggested by *Nishimura et al*. [2010b] suggests that flow bursts from the distant tail, which may be associated with localized reconnection, can trigger a near-Earth instability and subsequently lead to substorm onset. The quantitative analysis of the sequence of events and morphology of the magnetospheric and ionospheric signatures of a substorm is essential in order to fully resolve this controversy. This is inherently difficult using in situ spacecraft measurements of electromagnetic fields and plasma since one must infer the state of highly dynamic global nightside processes from a few single-point measurements. Ground-based observations of the ionosphere, with careful analysis, can provide a unique view of a much larger two-dimensional region linked to the entire nightside magnetosphere. In particular, the THEMIS all-sky imagers (ASIs) [*Mende et al*., 2008] provide the ability to diagnose the auroral morphology through the substorm growth and expansion phases and the ability to indirectly infer information about the processes which lead to the initiation of the substorm expansion phase [see, for example, *Rae et al*., 2010]. In this paper we present a novel technique with which to automatically identify a time interval and spatial location using optical all-sky imager (ASI) data that consistently identify the significant brightening and expansion of the aurora during the substorm expansion phase known as auroral breakup [*Akasofu*, 1964] using optical all-sky imager (ASI) data. We present an auroral breakup timing technique based on a quantitative algorithm applied to ASI data and not through visual identifications ostensibly "by eye" by an individual researcher.

Previous work to automatically and routinely identify substorm onset has largely concentrated on ground-based magnetometer observations of the impulsive Pi1 and Pi2 ultralow frequency (ULF) magnetic waves observed at substorm onset [*Jacobs et al*., 1964] that are highly correlated with auroral intensity [*Rae et al*., 2012] and may be used as a proxy for auroral substorm onset [*Sakurai and Saito*, 1976]. *Sutcliffe* [1997] trained a neural network to determine substorm onsets by identifying Pi2 pulsations at low-latitude ground-based magnetometer stations. Similarly, *Nose et al*. [1998] used a Meyer wavelet to automatically identify Pi2 pulsations at low-latitude ground-based magnetometer stations. While both *Sutcliffe* [1997] and *Nose et al*. [1998] were able to routinely identify Pi2 pulsations, the delay between auroral zone ULF waves and low-latitude ULF waves can be on the order of minutes, introducing additional timing uncertainties when observing ULF waves away from the onset location. Significantly, neither method is capable of identifying the ionospheric location of substorm onset.

Milling et al. [2008; see also *Murphy et al*., 2009] used a similar technique to that developed by *Nose et al*. [1998] to identify both the time and location of substorm onset using ground-based magnetometer observations of ULF waves in the auroral zone. These authors demonstrated that both the time and location of substorm onset could be determined by applying discrete wavelet transforms to the data from a network of magnetometers. While robust, the method described by *Milling et al*. [2008] required user input of a preidentified approximate time of the onset, thus making it difficult to use in large-scale statistical studies. Though ground-based magnetometer observations provide vital information for understanding substorm dynamics, routine identification of optical onsets would be an extremely valuable additional capability. In this paper we present a new technique using ground-based optical observations of the aurora from the THEMIS ASIs.

The auroral morphology through the substorm growth and expansion phases is one of the most well-defined observations of the substorm sequence. However, there is no consensus in the literature as to what constitutes the very first moment of a brightening or subsequent breakup. This is complicated by the fact that typically these phenomena are identified by eye, such that the chosen time of brightening and breakup can be dependent on the signal-to-noise in the measurement, the sensitivity of the instrument, and any automated normalization of the data.

We propose that a database of auroral breakup times generated via a reproducible automated algorithm will provide a more reliable basis for statistics with which to test hypotheses regarding the physical mechanisms responsible for triggering substorm expansion phase onset. This database will be analyzed in future work; in this paper, we describe the algorithm itself.

2. Automated Determination of Auroral Breakup

The first auroral indication of the onset of the substorm expansion phase is a sudden and localized brightening of the aurora [*Akasofu*, 1977]. This brightening can occur in a preexisting auroral arc [e.g., *Rae et al*.,

©2014. American Geophysical Union. All Rights Reserved.

2009b] or on a diffuse or newly formed auroral arc [e.g., *Rae et al*., 2009a]. The initial brightening is followed by auroral breakup and the poleward and azimuthal expansion of the aurora. Despite this rather simple definition of substorm onset, there is often no consensus as to what constitutes the initial time of auroral onset (compare for instance *Mende et al*. [2009], *Lui et al*. [2008], and *Nishimura et al*. [2010c]). In addition, instrumental and environmental noise detected by auroral cameras (for instance clouds and moon glow) can significantly influence any quantitative determination of auroral onset. In this section we describe an algorithm which identifies a period of rapid auroral brightening and expansion. This time naturally occurs immediately following auroral onset and describes the auroral breakup during the substorm expansion phase defined by *Akasofu* [1964] as "the most violent form of (auroral) display." Hence, we term this interval as the auroral breakup time or interval throughout the remainder of the manuscript. Our quantitative definition of the auroral breakup interval provides an unbiased method with which to routinely identify physically similar periods of auroral brightening that can be used in statistical studies.

In auroral cameras, the localized, rapid brightening of the expansion phase aurora is characterized by a rapid exponential growth in the intensity [e.g., *Voronkov et al*., 2003; *Rae et al*., 2012] and a rapid increase in time derivative of the intensity. In a dynamic power spectrum, these changes manifest as a sudden increase in power across a broad band of frequencies. In our new technique, the dynamic power spectrum of both the auroral intensity and the time derivative of the auroral intensity are used to define an auroral brightness parameter, denoted the brightening factor (*BF*), to automatically define a spatial window and time interval of auroral brightening for individual substorms.

For any time interval, the *BF* is calculated from the time-dependent smoothed average intensity $i(t)$ within a defined region (subwindow) of the field of view (FOV) of an individual THEMIS ASI and its time derivative $i'(t)$, where

$$i(t) = \mathrm{smooth}\left(\frac{\Sigma_x \Sigma_y C(x,y,t)}{\Delta x \Delta y}, \mathrm{spt}\right), \tag{1}$$

C is the ASI count rate for each individual pixel in the ASI FOV at a given time t, and spt is the number of points used for the smoothing. The area of the subwindow is Δx times Δy, such that $i(t)$ represents a normalized intensity within the subwindow. The power spectra of both $i(t)$ and $i'(t)$ are then calculated over a finite time interval Δt and stepped in time by δt to generate dynamic power spectra $I(f,t)$ and $I'(f,t)$. The dynamic power spectra are then summed over a configurable frequency range f providing the total power $J(t)$ and $J'(t)$ as a function of time.

$$J(t) = \sum_{f=a}^{b} I(f,t). \tag{2}$$

$$J'(t) = \sum_{f=a}^{b} I'(f,t). \tag{3}$$

In equations (2) and (3), a and b are constants specifying the frequency range over which the summed power $J(t)$ and $J'(t)$ are calculated. This frequency range can be tailored and optimized for specific applications such as the study of high-frequency changes in the aurora (i.e., flickering aurora) or low-frequency variations (e.g., long-period variations along the growth phase arc). The brightness factor *BF* is then defined as the product of J and J'

$$BF(t) = J(t)^n \times J'(t)^m \times s. \tag{4}$$

As the sign of $i(t)$ and $i'(t)$ is lost in the fast Fourier transform (FFT), s accounts for the slope (and hence sign) of both $i(t)$ and $i'(t)$. If either the slope of $i(t)$ or $i'(t)$ is negative, then $s = -1$, for all other values $s = 1$. This ensures that over the FFT interval Δt, a positive brightening factor corresponds to a brightening, rather than a dimming. In equation (4) the constants n and m are weighting factors such that the influence of the auroral intensity and temporal rate of change of intensity can be set individually. For the purpose of this manuscript we set n and m to unity, though we discuss the variation of *BF* with n and m below. We utilize the dynamic FFT and $J(t)$ and $J'(t)$ rather than $i(t)$ and $i'(t)$ to define *BF* because the FFT allows us to select frequency ranges of interest. If we were to use $i(t)$ and $i'(t)$, rather than J and J' to define *BF*, then the contribution of

©2014. American Geophysical Union. All Rights Reserved.

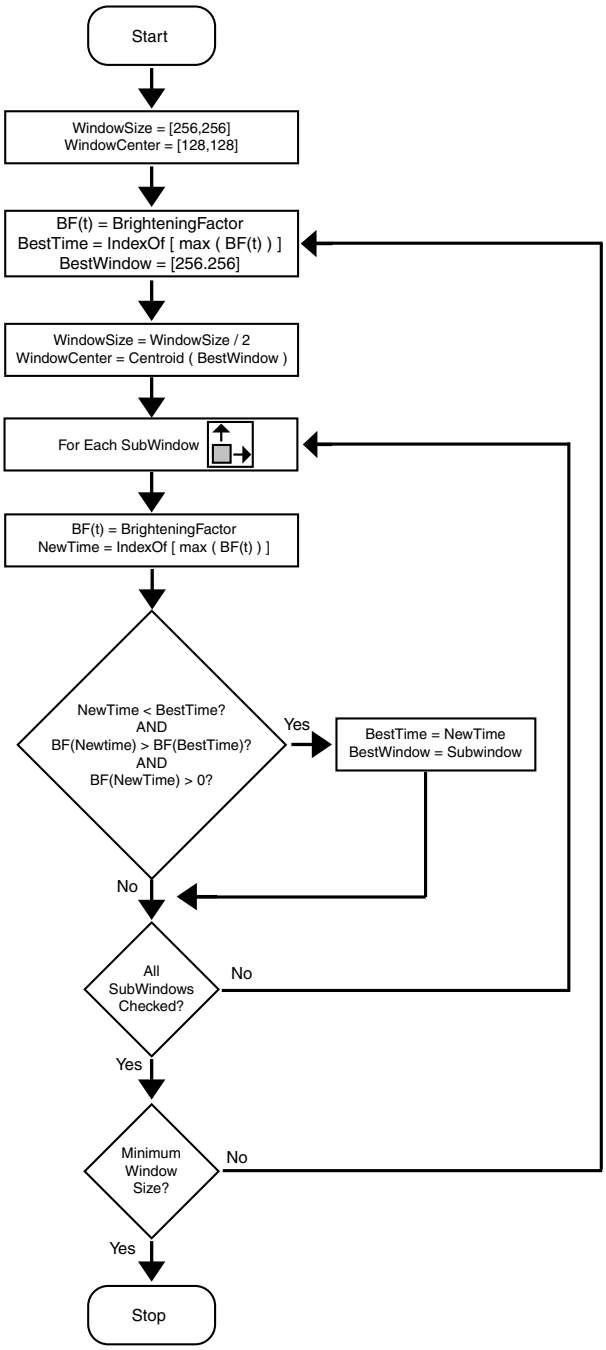

Figure 1. A description of the iterative process to refine the auroral onset time and location as defined by the brightening factor *BF*.

high-frequency variations, which may not lead to a continued brightening of the aurora, could provide an inaccurate identification of the auroral breakup interval. The utility of the FFT is illustrated in the next section.

Finally, the interval that contains auroral breakup is defined as the interval that provides the maximum value of $BF(t)$. These intervals are tagged to the time of the center of each FFT interval but should be understood to be an interval with a time uncertainty $(\Delta t/2) + \delta t$.

To demonstrate this concept, we use the THEMIS ASI data sets, which have a 3 s cadence and spatial resolution of 256 × 256 pixels. Initially, the interval containing auroral breakup is constrained using *BF* calculated over the entire 256 × 256 FOV. However, a refined interval and location can be determined by calculating *BF* in progressively smaller subwindows of the imager FOV. Figure 1 illustrates an iterative scheme whereby the use of sequentially smaller subwindows allows a refinement in both the time and location of the auroral breakup interval. Once the initial estimate of auroral breakup time is obtained from the full 256 × 256 FOV, the analysis window is shrunk by a factor of 2 to produce a 128 × 128 subwindow in the bottom left quarter of the total 256 × 256 image, and a new $BF(t)$ is calculated for this subwindow. A new breakup time interval is identified if the maximum value of $BF(t)$ over the subwindow is greater than that over the full 256 × 256 window, and the time of the subwindow maximum of $BF(t)$ is earlier than that identified previously from the larger window.

In order to identify more specifically the auroral breakup location, the subwindow is stepped across the field of view of the ASI to seek the location that gives the largest and earliest auroral brightening. The 128 × 128 subwindow is stepped across the *x* and *y* directions, first in *x* and then in *y*, by half the subwindow width, and at each iteration a new $BF(t)$ and related breakup interval are calculated. The breakup window (BW) is then determined to be the subwindow with the largest maximum value of $BF(t)$, remembering that the maximum of the new $BF(t)$ must be greater than that defined in the previous 256 × 256 window and occur during the same time interval or earlier.

Once an optimal breakup interval and location are identified for the 128 × 128 size subwindow, the BW is recentered in preparation for the next level of iteration. The location of the approximate centroid of auroral intensity at the end of the breakup interval is determined by computing the pixel in *x* with the largest *y*

©2014. American Geophysical Union. All Rights Reserved.

Table 1. Auroral Breakup Intervals Times for Four Signals With Varying Noise Levels

Source	Auroral Breakup Intervals (Seconds Past $t_0 \pm 7.5$ s)
Test signal 15% noise	675–735
Test signal 210% noise	675–735
Test signal 315% noise	675–735
Test signal 420% noise	660–690

integrated intensity, and the pixel in y corresponding to the integrated x intensity, within the BW. To seek an increasingly refined location for auroral breakup, the analysis subwindow is repeatedly shrunk by a factor of 2 in both axes, and the process is repeated within each new BW. The process of shrinking the analysis subwindow and stepping through to refine both the breakup interval and location is repeated until a minimum window size is reached. The final auroral breakup interval is hence determined from the subwindow with the largest maximum value of $BF(t)$ during the earliest breakup interval. Together, equations (1)–(4) and Figure 1 characterize the steps the algorithm uses for automatic identification of auroral breakup interval and location.

Auroral breakup occurs on minute timescales [*Akasofu*, 1964] so prior to the analysis we smooth the auroral data over five points (15 s). The dynamic FFT time interval is set to $\Delta t = 1$ min (20 data points) with a step size δt equal to 25% of the FFT window (15 s). Additionally, both m and n are set to 1, and the total power in equations (2) and (3) is determined by summing over all but the zero frequency bin. The minimum subwindow which is to be analyzed is set to 32×32 pixels, ensuring sufficient expansion of the aurora within the field of view. In general, any of these parameters can be changed as appropriate for specific target studies. For instance, the dynamic FFT time interval and step size can be altered for specific instrumentation with different cadences and temporal resolutions. The values of m and n, and a and b, can also be adjusted to identify specific auroral features. For example, if one was interested in the brightening of a preexisting arc the value of n could be made larger than m (so long as $J(t)$ remains larger than one). On the other hand, if auroral dynamics including auroral beads [*Rae et al*., 2009a] or pulsating aurora [*Nishimura et al*., 2010a] were to be studied, then the value of m could be increased to weight $J'(t)$ more heavily than $J(t)$ (again ensuring $J'(t)$ remains larger than one) and the range of a and b could be truncated to include only the frequencies associated with auroral beads and pulsating aurora. In this paper though, we focus on the auroral algorithm as applied to the rapid brightening that occurs just after the substorm expansion phase onset.

It is important to note that the initial auroral brightening at substorm onset is a poorly defined event, and no specific criteria or thresholds are used consistently in the literature to describe the phenomenon, e.g., there is no agreed measure of absolute brightness increase, relative brightness compared to dark sky, relative brightness compared to average sky, relative brightness compared to nearby sky, the physical size of the brightening area, or the length of time over which the auroral should brighten. Even assuming these criteria are applied consistently, the "initial" brightening is dependent on background noise, both instrumental and environmental, introducing systematic errors into any definition of the initial brightening. For example, a dim but continuously brightening auroral feature can have a later initial brightening if observed in a bright sky than if observed in a dark sky since the bright sky will mask the early and small amplitude brightening.

The algorithm described in this paper is not immune to the effects listed above. However, it is more robust than traditional methods because it consistently identifies physically similar periods of auroral brightening following substorm onset which can be meaningfully compared between events. It is clear from the preceding discussion that the earliest detection of the rapid increase in auroral brightness does not necessarily correspond to the earliest time of an increase in particle precipitation and may depend on instrument or environmental noise. In order to demonstrate the robustness of the algorithm we have considered a test auroral signal with various noise levels. The test signal is constructed from a two-dimensional Gaussian which grows exponentially in time until it reaches a peak amplitude. A background of random noise with an amplitude of 5, 10, 15, and 20% of the peak amplitude of the Gaussian is then added to create the test signal. Movie S1 in the supporting information is an animation of the four test signals; the white box identifies both the breakup time and location. In each of the four test cases the brightness function identifies the same interval of auroral brightening within the uncertainty inherent in the algorithm, demonstrating the robustness of the algorithm in the presence of increasing noise levels. Note that the purpose of the test signal is to demonstrate the robustness of the algorithm in the presence of different noise levels. The time intervals are summarized in Table 1.

©2014. American Geophysical Union. All Rights Reserved.

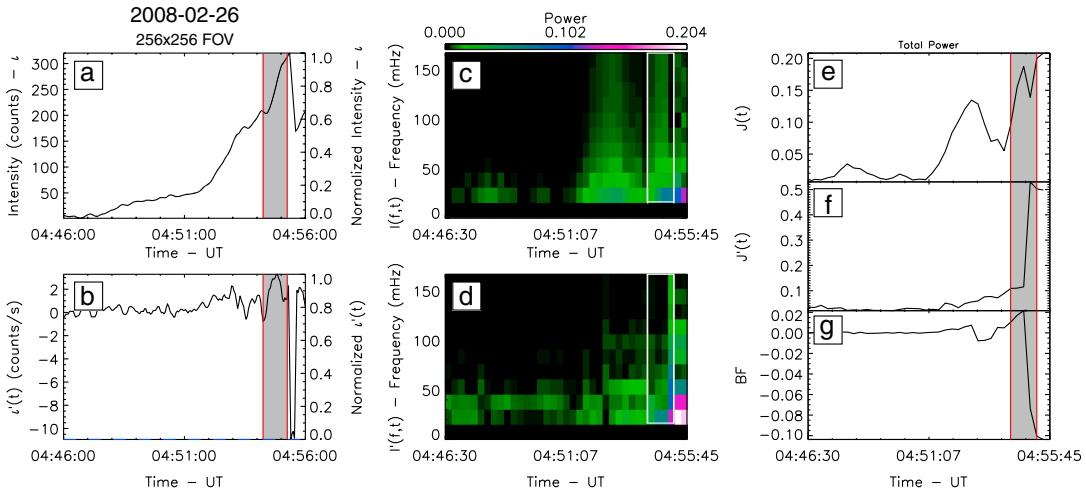

Figure 2. The initial iteration of the determination of the brightness factor *BF* and auroral breakup interval for the 26 February 2008 substorm observed by the Gillam ASI. (a) $i(t)$ and (b) $i'(t)$. The shaded region identifies the initial breakup interval. The dynamic power of (c) $i(t)$ and (d) $i'(t)$. The white box indicates the frequency range used to define $J(t)$ and $J'(t)$ as well as the time interval of auroral breakup. (e) $J(t)$, (f) $J'(t)$, and (g) *BF*. The shaded box in Figures 2e–2g indicates the initial breakup interval.

In the next section we demonstrate the utility of the algorithm described above by comparing the breakup interval as determined by the *BF* and iterative stepping scheme with auroral onset times previously published in the literature.

3. Demonstration of Algorithm

For the purpose of a comparison between our results and previously published timings we consider three publications, *Angelopoulos et al*. [2008], *Murphy et al*. [2012], and *Nishimura et al*. [2010b], all of whom use the THEMIS ASIs to characterize auroral onset. Note that both *Angelopoulos et al*. [2008] and *Murphy et al*. [2012] each consider a single substorm whereas *Nishimura et al*. [2010b] provide a list of 240 auroral brightenings; for the latter case we will first select a single auroral brightening from the list for case study comparison. Finally, we present a statistical comparison of all the onset times presented in the *Nishimura et al*. [2010b] list and the center of the breakup intervals determined automatically by the algorithm presented in this manuscript.

3.1. Case Studies

Angelopoulos et al. [2008] calculate an auroral onset time by identifying the inflection point in the integrated auroral intensity *f* from the northern half of the Gillam ASIs FOV (i.e., essentially the maximum of $i'(t)$ as used in this study). The auroral onset of the substorm on 26 February 2008 is determined to be at 04:57:39 UT.

For a comparison between our technique and that used by others, the initial time series of $BF(t)$ is first calculated from the entire FOV of a single ASI using a 10 min interval centered on the onset time provided independently in the literature. Once an initial breakup time t_0 (the center of breakup interval) is determined from the whole 256 × 256 FOV, $BF(t)$ is then calculated in each of the subwindows in the iterative stepping scheme from an interval defined by t_0 10 min to t_0. The shifting of the time series by 10 min allows the algorithm to search for earlier auroral brightening in successively smaller subwindows assuming that auroral brightenings at smaller scales will precede the initial large-scale auroral brightening identified in the 256 × 256 FOV.

Figure 2 shows an overview of the execution of the algorithm and the determination of $BF(t)$ in the initial iteration taking into account the entire 256 × 256 FOV of the Gillam ASI. An initial estimate of the breakup interval is determined from the FFT window containing the maximum in $BF(t)$, Figure 2g, at 04:54:45 UT and will be reported as 04:54:15–04:55:15 UT ± 7.5 s.

Figures 2a and 2b show the integrated intensity $i(t)$ and the time derivative of intensity $i'(t)$, respectively, for the initial iteration and calculated across the entire 256 × 256 ASI window. The shaded region in Figures 2a

©2014. American Geophysical Union. All Rights Reserved.

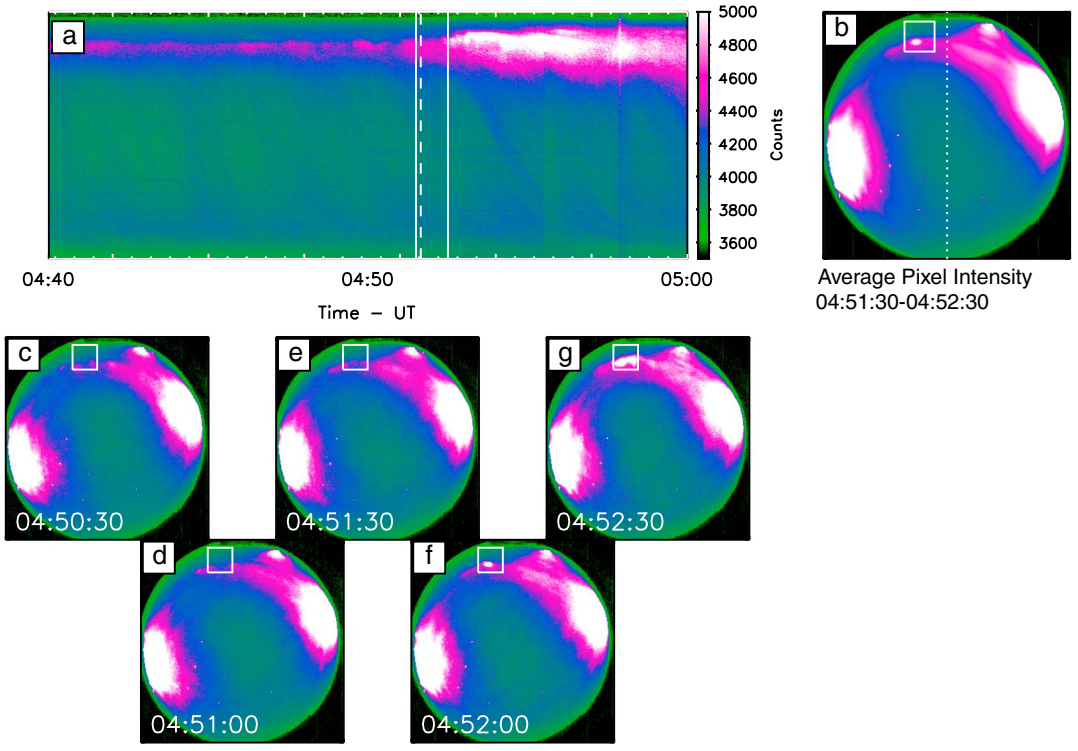

Figure 3. A summary of the auroral onset and breakup interval from the Gillam ASI on 26 February 2008. (a) A keogram showing the onset time determined by *Angelopoulos et al.* [2008] using a dashed line at 04:51:39 UT and the refined breakup interval determined by the auroral algorithm using solid lines at 04:51:30–04:52:30 UT. (b) The average ASI intensity throughout the breakup interval, 05:51:30–05:52:30 UT. (c–g) Three second images at 30 s time steps surrounding the onset time. The white box in Figures 3b–3g marks the auroral breakup location.

and 2b indicates the initial identification of the breakup interval. Note the sudden increase in both $i(t)$ and $i'(t)$ directly after the independently defined onset time from *Angelopoulos et al.* [2008]. The rapid increases in brightness associated with breakup show a clear increase in power across the entire frequency band in Figures 2c and 2d. Note both $i(t)$ and $i'(t)$ show evidence of rapid fluctuations not associated with the auroral breakup. These rapid fluctuations further demonstrate the utility of using the dynamic FFT to define *BF* rather than simply the time series. The FFT accounts for variations across all frequencies and allows the general trend of $i(t)$ and $i'(t)$ to be identified, i.e., an increase in $i(t)$ and $i'(t)$ over a period of time. If we were to consider only the time series of $i(t)$ and $i'(t)$ to define *BF*, then rapid fluctuations in both $i(t)$ and $i'(t)$ may lead to a discrete peak in $BF(t)$ but not a continued and expansive brightening, leading to the possible misidentification of auroral breakup. The white boxes in Figures 2c and 2d mark the breakup interval and the frequency range used to define $J(t)$ and $J'(t)$. Finally, Figures 2e–2g show the total power $J(t)$ and $J'(t)$ and the brightening factor $BF(t)$, respectively.

Once the initial breakup interval for examination is defined, the iterative stepping scheme considers a series of smaller subwindows to refine the breakup interval and location as described in section 2. The 10 min preceding the breakup interval is now used to evaluate each subsequent subwindow, i.e., 04:45–04:55 UT. Movie S2 in the supporting information illustrates the full implementation of the auroral algorithm, and Figure 3 illustrates the final breakup interval and location determined from the algorithm.

Figure 3a is a keogram taken from the center of the FOV of the Gillam ASI. The dashed vertical line marks the onset time determined by *Angelopoulos et al.* [2008] at 04:51:39 UT, and the solid lines mark the final breakup interval determined by the automated algorithm described here at 04:51:30–04:52:30 UT ± 7.5 s. Figure 3b shows the auroral brightness of the Gillam ASI where the intensity at each pixel has been averaged over the 1 min Δt window. The white box denotes the location of auroral breakup determined by the algorithm, and the vertical line is the FOV of the keogram. Note in particular the localized brightening in the breakup region. Figures 3c–3g are five snapshots from the Gillam ASI, 30 s apart, starting 1 min prior to the beginning of the breakup interval as determined by the algorithm. Note that before the breakup interval, in Figures 3c and 3d, there

©2014. American Geophysical Union. All Rights Reserved.

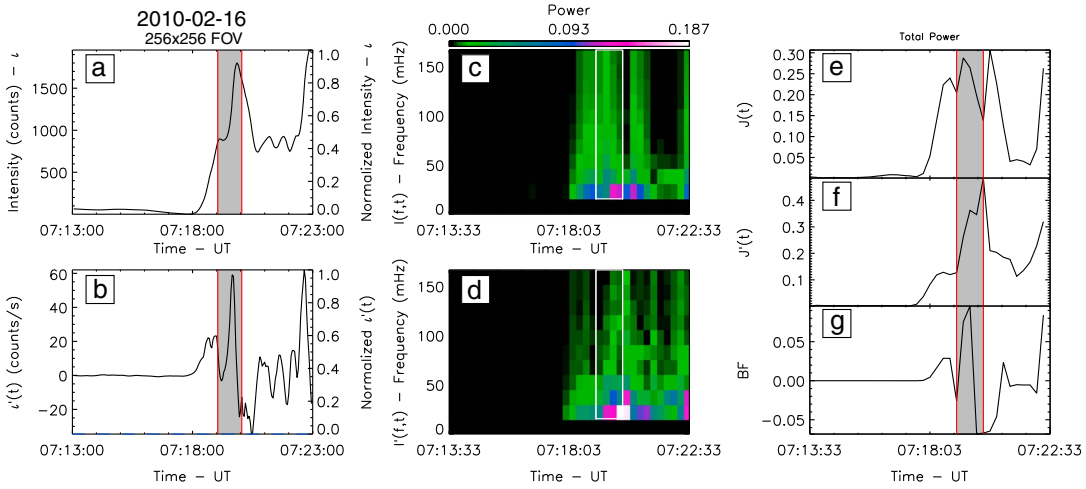

Figure 4. The initial iteration of the brightness factor for the substorm on 16 February 2012 from the Fort Simpson ASI, in the same format as Figure 2.

is little auroral activity and through the breakup interval, in Figures 3e–3g, there is an obvious brightening and expansion of the auroral emission within the region identified by the algorithm. Movie S3 in the supporting information shows the auroral dynamics through the substorm expansion phase during this event; the white box denotes the location of auroral breakup and turns red at the beginning of the algorithmically determined breakup interval at 04:51:30 UT. In summary, the auroral algorithm clearly identifies the breakup interval at the start of the substorm expansion phase in the Gillam ASI and that the onset time identified by *Angelopoulos et al.* [2008] was within this interval (including its uncertainty), despite the presence of clouds and moon glow within this period.

Figure 4 (in the same format as Figure 2) shows the calculation of $BF(t)$ in the full 256 × 256 FOV in the Fort Simpson ASI for the substorm characterized by *Murphy et al.* [2012]. Similar to the previous event, Figures 4a and 4b show a rapid increase in $i(t)$ and $i'(t)$, respectively, during the auroral breakup interval 07:19:03–07:20:03 UT ± 7.5 s (vertical line). These rapid increases are identified in the dynamic FFT by a sharp increase in power across the entire frequency spectrum, Figures 4c and 4d. Figures 4e–4g characterize the total integrated power $J(t)$, the change in total integrated power $J'(t)$, and the brightness factor $BF(t)$, respectively. The full implementation of the algorithm and the iterative stepping scheme is illustrated in Movie S4 in the supporting information. The final auroral breakup interval is determined to be (07:17:51–07:18:51) UT ± 7.5 s. The onset time at 07:18:30 UT, determined by eye in *Murphy et al.* [2012], lies within this breakup interval.

The agreement between the breakup interval defined by the auroral algorithm and the onset time defined by *Murphy et al.* [2012] is clearly illustrated in Figure 5 and Movie S5 in the supporting information. Figure 5 shows a summary of the substorm and the breakup interval defined by the algorithm for the 16 February 2010 substorm in the same format as Figure 3. Movie S5 in the supporting information shows the auroral dynamics from the Fort Simpson ASI during the substorm expansion phase on 16 February 2010 in the same format as Movie S3.

Finally, we examine a substorm on 11 February 2008, which is part of a list of substorms and auroral intensifications identified by *Nishimura et al.* [2010b]. *Nishimura et al.* [2010b] identify the auroral onset at 04:27 UT. Note that although the THEMIS ASIs have a 3 s resolution, all auroral onset times in *Nishimura et al.* [2010b] are defined to 1 min time resolution; thus, for the purpose of comparison we assume an error of ± 1 min in all onsets provided by *Nishimura et al.* [2010b].

Figure 6 (in the same format as Figure 2) shows the initial determination of auroral breakup for the 11 February 2008 substorm from the Sanikiluaq ASI using the full 256 × 256 FOV. The initial breakup interval is defined by the increases in both $i(t)$ and $i'(t)$ leading to a peak in $BF(t)$ at (04:27:48–04:28:48) UT (vertical line). Movie S6 provides a movie of the execution of the auroral algorithm for 11 February 2008. After the initial identification of the breakup interval, Movie S6 shows that when the auroral FOV is reduced, no peak in the brightening factor is observed. In this case the successive iterations of the algorithm refine the spatial location of auroral brightening but provide no refinement in time. The refined breakup interval and location are shown in Figure 7. After the iterative stepping process, the refined breakup interval is (04:27:37–04:28:36) UT ± 7.5 which overlaps with the

©2014. American Geophysical Union. All Rights Reserved.

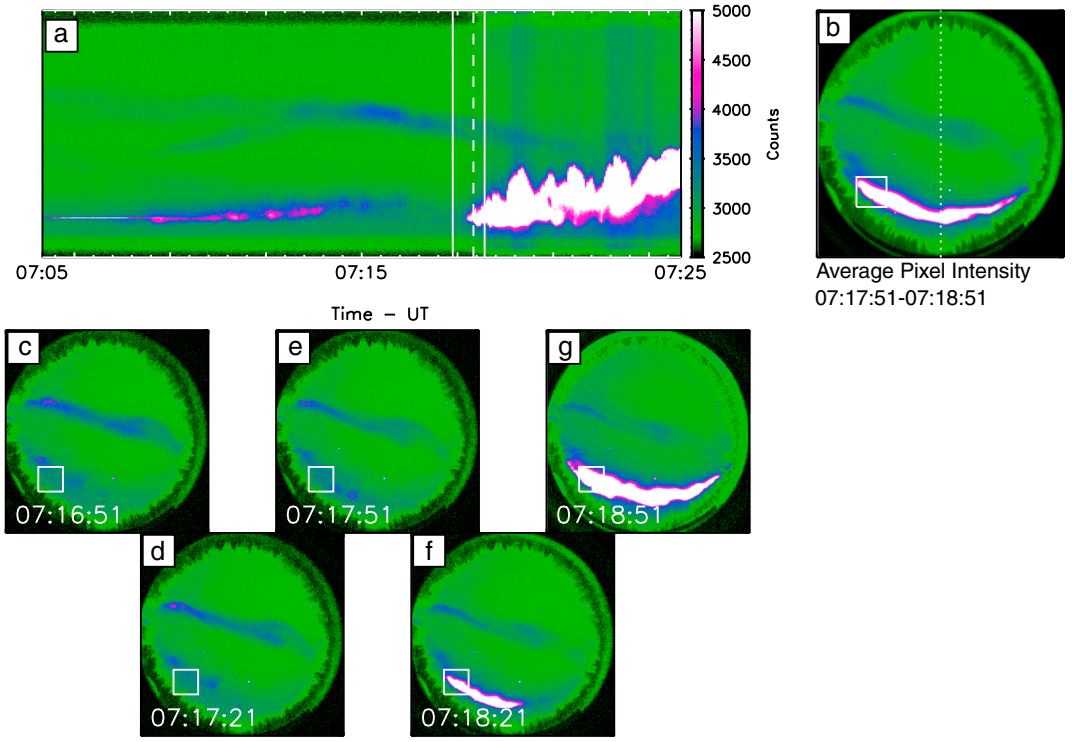

Figure 5. (a–f) A summary of the onset and breakup interval from the Fort Simpson ASI on 16 February 2012 in the same format as Figure 3. The dashed line in Figure 5a marks auroral onset defined by *Murphy et al.* [2012] at 07:18:30 UT, and the solid lines mark the breakup interval defined by the auroral algorithm, 07:17:51–07:18:51 UT.

range of uncertainty in the *Nishimura et al.* [2010b] onset of 04:27 UT ± 1 min. The dark bar in Figure 7a shows the 1 min uncertainty associated with the *Nishimura et al.* [2010b] onset times.

A summary of the breakup interval as determined by the auroral algorithm and *Nishimura et al.* [2010b] as well as the auroral dynamics are shown in Figure 7 (in the same format as Figure 3) and Movie S7 in the supporting information. The grey box in Figure 7a shows the uncertainty in the onset time from *Nishimura et al.* [2010b].

3.2. Statistical Comparison

In this section we compare 240 substorms and auroral onset times in *Nishimura et al.* [2010b] with the breakup intervals defined by the algorithm described in this paper. In addition, we perform a small parameter search

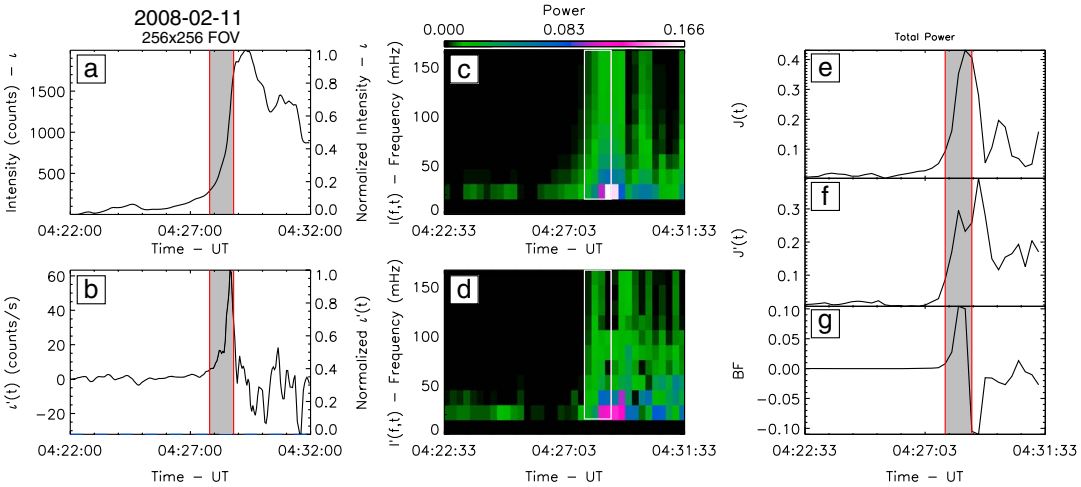

Figure 6. The initial iteration of the brightness factor for the substorm on 11 February 2008 from the Sanikiluaq ASI, in the same format as Figure 2.

©2014. American Geophysical Union. All Rights Reserved.

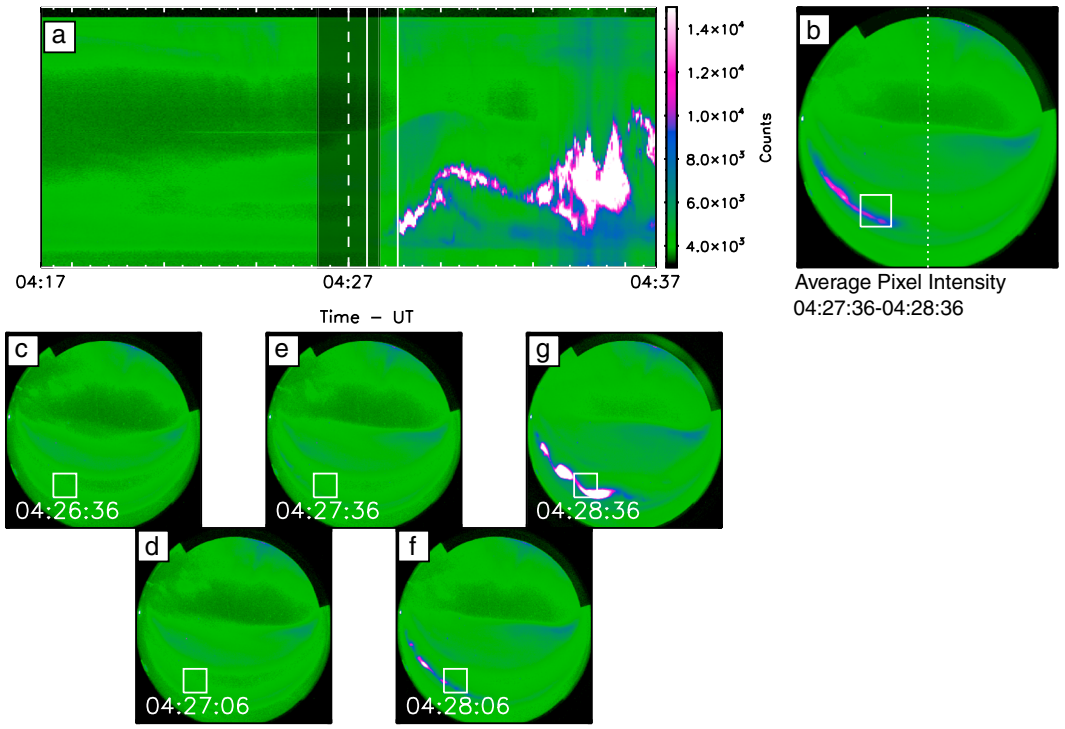

Figure 7. (a–f) A summary of the onset and breakup interval from the Sanikiluaq ASI on 11 February 2008 in the same format as Figure 3. The dashed line in Figure 7a marks auroral onset defined by *Nishimura et al.* [2010c] at 04:27 UT with the 1 min uncertainty (shaded region), and the solid lines mark the breakup interval defined by the auroral algorithm, 04:27:48–04:28:48 UT.

over the values of m, n, a, b, and the window start time. For example, we experiment with investigating the time intervals between t_0 8 min and $t_0 + 2$, rather than between t_0 10 min and t_0, for the iterative part of the search so that there is a 2 min overlap between the initial interval and the 10 min window used to make subsequent iterations. This allows for any potential misidentification of the initial breakup interval.

To directly compare the time interval identified by the algorithm with those identified by *Nishimura et al.* [2010b] we use the middle of the breakup window defined by Δt to define a breakup time rather than a breakup interval and assume an added uncertainty of ±30 s. This makes the total uncertainty from the algorithm ±7.5 s (from the 15 s step size) plus ±30 s (from the FFT window size) for a total of ± 37.5 s. As noted in previous sections, the uncertainty in the onset time defined by *Nishimura et al.* [2010b] is assumed to be ±60 s. With these uncertainties, the timings can be up to ±97.5 s apart and still correspond to the same event. We also note that there are auroral brightenings within the *Nishimura et al.* [2010b] list which occur as little as 3 min apart. This is shorter than the window length used by the algorithm (10 min); thus, we have considered the *Nishimura et al.* [2010b] database two ways: including (i) all onsets in the list and (ii) only isolated onsets defined as those which are separated by at least 30 min from any other onset.

Figure 8 shows the distribution of the difference between the center of our breakup intervals as determined by our auroral algorithm (T_A) and the onset times provided in the *Nishimura et al.* [2010b] list (T_N) for all events (Figure 8a) and isolated events (Figure 8b). A negative difference indicates the *Nishimura et al.* [2010b] onset follows that defined by the auroral algorithm. Evident in Figure 8 is that T_A-T_N is clustered just above zero. When considering all substorms, Figure 8a, 49% of the event timings agree within the uncertainty. When considering only isolated substorms, Figure 8b, 48% of events agree within the uncertainty. The median of the distribution lies at 90 s, within the combined uncertainty, clearly demonstrating the utility of the algorithm in identifying auroral brightenings during the substorm expansion phase. We do note that discrepancies exist and discuss this in section 5.

Figure 9 shows the distribution of T_A-T_N for five different sets of algorithm parameters during all events (Figure 9 (left)) and isolated events (Figure 9 (right)). The first row is the distribution of events where a

©2014. American Geophysical Union. All Rights Reserved.

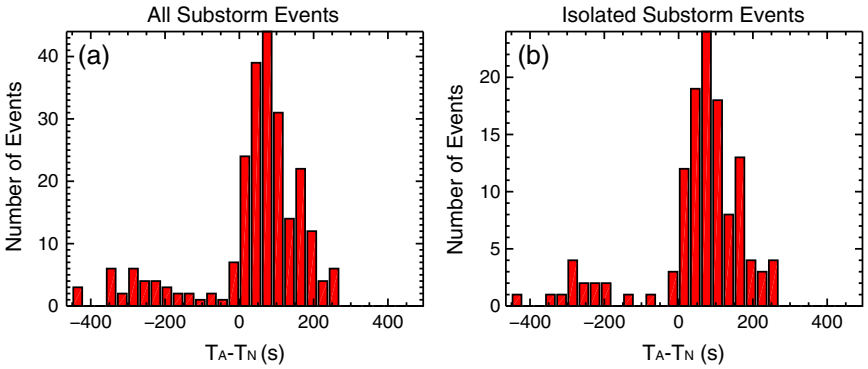

Figure 8. A comparison of timings for all substorms from *Nishimura et al.* [2010b]. In both panels the *x* axis is the time difference between the center of the auroral breakup interval identified using our algorithm and the onset time defined in *Nishimura et al.* [2010b], T_A-T_N in seconds. (a) All substorms characterized by *Nishimura et al.* [2010b]. (b) Isolated substorms from the *Nishimura et al.* [2010b] substorm list.

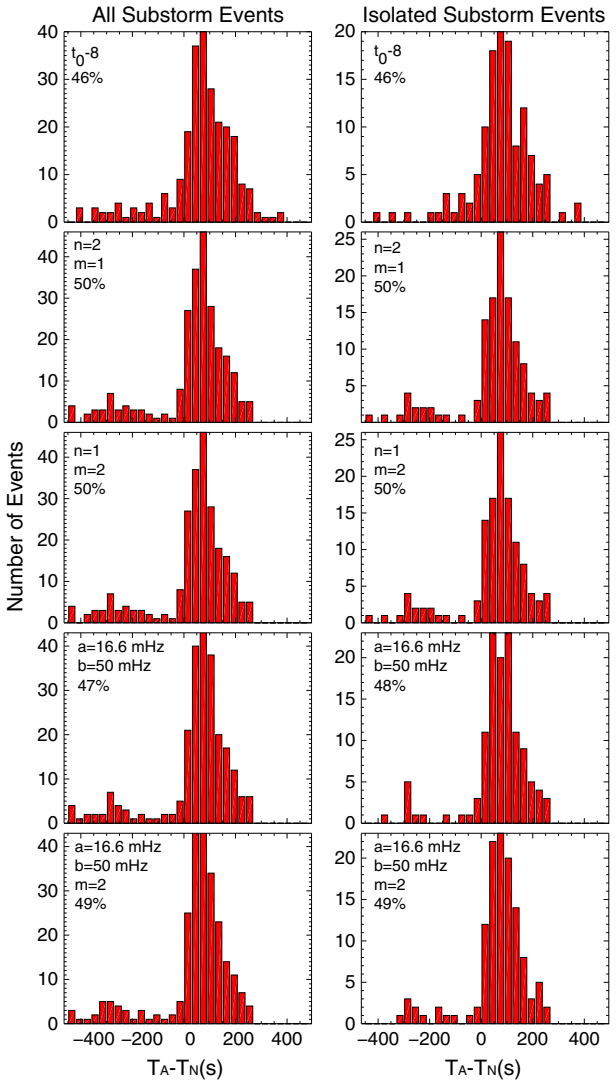

Figure 9. A comparison of the timing for all (left) aurora events and (right) isolated events from *Nishimura et al.* [2010b] for various adjustable parameters in the auroral algorithm. The figure is in the same format as Figure 8. The changed parameter is shown in the top left corner; all other parameters are kept the same. The percentages indicate the number of events within the uncertainty.

10 min interval defined by t_0 8 min to $t_0 + 2$ is used in the subwindow searches (t_0 is the center of the initial auroral breakup interval defined over the full 256 × 256 pixel ASI window). The second row is the distribution of events for $n = 2$ and $m = 1$. The third row shows the distribution of the differences for $n = 1$ and $m = 2$. The fourth row looks at specific frequency range in determining $J(t)$ and $J'(t)$. Typically, substorm expansion phase onset is associated with ultralow frequency (ULF) waves in the Pi1 (1–40 s) and Pi2 (40–150 s) wavebands [*Jacobs et al.*, 1964]. Recent work has shown that the initial wave perturbations observed by ground-based magnetometers and auroral imagers have periods of 24–96 s [*Murphy et al.*, 2009; *Rae et al.*, 2009a]. As such, to concentrate on wave activity, we have looked at the difference in auroral breakup times when considering the frequency range 16.67–50 mHz (20–60 s). This is the frequency range available in a 1 min FFT window, with a 16.67 mHz resolution, which spans the 24–96 s period band of ULF waves observed at substorm onset. The final row of Figure 9 uses the 16.6–50 mHz frequency range and a value of $m = 2$. The parameters used for each distribution are shown in the top left of each panel along with the percentage of events that agree with Nishimura et al.'s timings within the 97.5 s uncertainty.

In general, each histogram shows good agreement; 46–50% of events fall within the uncertainty between the center of the

©2014. American Geophysical Union. All Rights Reserved.

interval determined by the algorithm and the onset time determined by *Nishimura et al.* [2010b]. In each case the histograms peak at 30–90 s. The algorithm necessarily defines a time interval after auroral onset and so we expect the difference to peak at positive values rather than negative values. The smallest percentage of events within uncertainty is when the t_0 8 to $t_0 + 2$ min interval is used for subwindow searches, Figure 9 (first row), about 3% (or seven events) less than if we were to use an interval from t_0 10 min to t_0 (Figure 8a). The best agreement is achieved when either n or m is set to 2, Figure 9 (second and third rows), where 50% of the events fall within the uncertainty. In all cases, the peak of the distribution lies within in the uncertainty demonstrating the robustness of the algorithm and the utility for identifying auroral breakup in future studies.

4. Scientific Applications

In this manuscript we have introduced a novel and automated technique for the accurate determination of the time and location of the auroral breakup that immediately follows substorm onset. Historically, auroral onset has typically been defined through a visual inspection of the auroral dynamics during the late growth phase and early expansion phase. This can introduce a number of unavoidable human biases based on the visual inspection of a complex and dynamic data set. It also makes it difficult to undertake quantitative large-scale statistical studies of auroral onset as it is impractical to have a single human observer evaluate every possible event in precisely the same way. More importantly, the necessarily qualitative assessment made by different observers makes quantitative comparison between the results from different studies difficult or impossible. The routine identification of auroral brightenings plus the definition of a quantitative parameter, the brightening factor *BF*, provides a reliable, and most importantly, reproducible foundation on which to do statistical studies of the aurora. Specifically, the algorithm described here will enable statistical characterization of the time delay between ionospheric signatures of the expansion phase, and magnetospheric signatures of substorm expansion phase, such as the near-Earth depolarization of the magnetic field. Such a quantitative comparison should make it possible to determine the most probable sequence of events during the substorm expansion phase. The auroral breakup location as determined by the algorithm presented here (i.e., the white boxes in Figures 3, 5, and 7) can also be compared to the location of the open-closed field line boundary defined by the electron aurora [*Blanchard et al*., 1995] and to the location of the transition between tail and dipolar magnetic field configurations defined by the proton aurora [*Samson et al*., 1992] in order to try to determine the location of the magnetospheric counterpart of auroral onset. In addition, the algorithm can be run on any 2-D auroral measurements, including spectrally resolved auroral imagers, in situ auroral imagers such as Polar UV Imager [*Torr et al*., 1995], and Image FUV [*Mende et al*., 2000; *Frey et al*., 2003] to characterize the initial auroral expansion from global images. Utilizing multispectral cameras, the algorithm can be used to determine whether there are any differences in the expansion of the aurora at different wavelengths and further probe the energies of electrons in the initial auroral expansion. Suitable adjustments to the algorithm may be used to determine whether all substorms have a dimming of the aurora in a region conjugate to, but just prior to, auroral onset [*Pellinen and Heikkila*, 1978; *Murphy et al*., 2012].

Finally, it will be interesting to investigate whether *BF* is a useful proxy for, say, the size of a substorm and the amount of energy that is deposited in the ionosphere during the expansion phase. This will be investigated in future work.

5. Discussion and Conclusions

Auroral substorm onset time and location are characterized by a sudden brightening of the aurora followed by poleward motion and auroral breakup and development of the westward traveling surge [*Akasofu*, 1977]. Quantitatively, this means that the aurora increases in brightness and the rate of change of brightness also increases. Utilizing the product of the auroral intensity and rate of change of intensity *BF*, we have developed an algorithm which first defines an auroral breakup interval based upon the integrated brightness of the entire FOV of an auroral imager and then iteratively refines this breakup time interval using successively smaller subwindows of the FOV. The algorithm has been compared with the results from three independent studies [*Angelopoulos et al*., 2008; *Nishimura et al*., 2010c; *Murphy et al*., 2012] which identify auroral substorm onset time using the same auroral data. In all three cases, the algorithm identifies a breakup interval within the defined timing uncertainty. Table 2 summarizes the auroral onset times from the three studies and the auroral breakup intervals determined from the algorithm set out in this paper.

©2014. American Geophysical Union. All Rights Reserved.

Table 2. Comparison of Auroral Onset Times Defined in the Literature and Those Determined by the Auroral Algorithm

Source[a]	Literature Onset Time (UT)	Algorithm Breakup Interval (±7.5 s) (UT)
Angelopoulos et al. [2008] 26/02/2008	04:51:39	04:51:30–04:52:30
Murphy et al. [2012] 16/02/2010	07:18:30	07:17:51–07:18:51
Nishimura et al. [2010b] 11/02/2008	04:27 ± 1 min	04:27:48–04:28:48

[a]Dates are formatted as day/month/year.

The algorithm was compared to an independent list of 240 substorm onsets and auroral intensifications from *Nishimura et al.* [2010b]. We have demonstrated that in up to 50% of events, the algorithm identifies an auroral breakup interval within the uncertainty of previously published substorm onset time results. We do, however, note that large discrepancies exist for some events between the onset time defined by *Nishimura et al.* [2010b] and the breakup interval defined by the auroral algorithm presented here. The timing discrepancies for such events are, in general, explained by the result of light pollution within the ASI FOV, causing an erroneous identification of a substorm. Light pollution can include automobiles at the edge of the FOV, moon glow, and smoke stacks within the FOV of the ASI (see, for example, the data from the Kuujjuaq ASI). The future statistical studies that will be undertaken using the automated auroral algorithm presented here will utilize those THEMIS ASI sites which have significantly less light pollution.

The use of the FFT in the automated algorithm necessarily defines an interval window length Δt, rather than a discrete time. For comparison to the timings reported in *Nishimura et al.* [2010b], we use the center of the breakup interval (the period of rapid brightening), and thus, we expect to identify times later than those in *Nishimura* [2010b], who appear to have identified the "beginning" of the brightening associated with substorm onset. The time differences illustrated in Figures 8 and 9 are therefore expected to be skewed toward positive values. It is interesting to note that in each of the comparisons in section 3.2, the histograms peak within the accepted uncertainty, indicating that the auroral brightening that occurs soon after substorm expansion phase onset is indeed very rapid and occurs close to the time identified by eye as the first evidence of substorm auroral brightening. The algorithm provides a robust and unbiased mechanism for routinely and quantitatively identifying the timing and location of auroral breakup and offers a benchmark for future research and statistical analyses. Refinement of the algorithm can occur over time and the implementation can change for specific studies, such as the choice of the a, b, m, and n parameters in equations (2), (3), and (4). A small parameter sweep, presented in Figure 9, suggests that a choice of m or $n = 2$ provides a good basis for the identification of the peak in auroral intensity and brightening during the substorm expansion phase. This is not unexpected as these parameters will, in general, steepen the curves of $J(t)$ and $J'(t)$ making the peak in either time series more pronounced. It is important to note that as presented herein, the algorithm requires an initial identification of a substorm in order to specify a well-defined interval and location for the initial substorm brightening. Future work will identify periods of poleward moving aurora which have a total brightness exceeding a predefined threshold in order to identify periods of substorm activity from "unseen" data. The poleward motion is characteristic of substorm onset, and the selection of a quantitative threshold in total brightness provides a repeatable and consistent basis with which to characterize auroral breakup. This extension of the algorithm will provide a quantitative foundation to statistically characterize the initial auroral brightening for future studies. Overall, the algorithm presented here offers a powerful and configurable quantitative technique for the automated characterization of the time and location of auroral features, including the rapid brightening near the beginning of the auroral substorm expansion phase.

Acknowledgments

K.R.M. is funded by an Alberta Innovates Graduate Scholarship. I.R.M is supported by a Discovery Grant from NSERC. I.J.R. and C.E.J.W were funded by the Canadian Space Agency (CSA). We acknowledge NASA contract NAS5-02099 and V. Angelopoulos for use of data from the THEMIS Mission and NSF support for GIMNAST through grant AGS-1004736. Specifically, we thank S. Mende and E. Donovan for use of the THEMIS ASI data. Deployment and data retrieval of the THEMIS ASIs were partly supported by CSA contract 9F007-046101 to the University of Calgary.

Robert Lysak thanks Larry Lyons and an anonymous reviewer for their assistance in evaluating this paper.

References

Akasofu, S. I. (1964), The development of the auroral substorm, *Planet. Space Sci.*, *12*(4), 273–282, doi:10.1016/0032-0633(64)90151-5.

Akasofu, S. I. (1977), *Physics of Magnetospheric Substorms*, D. Reidel Publishing Company, Dordrecht, Netherlands.

Angelopoulos, V. (2008), The THEMIS mission, *Space Sci. Rev.*, *141*, 4–34.

Angelopoulos, V., et al. (2008), Tail reconnection triggering substorm onset, *Science*, *321*(5891), 931–935, doi:10.1126/science.1160495.

Angelopoulos, V., et al. (2009), Response to comment on "Tail reconnection triggering substorm onset", *Science*, *324*(5933), pp. 1391.

Aubry, M. P., and R. L. McPherron (1971), Magnetotail changes in relation to the solar wind magnetic field and magnetospheric substorms, *J. Geophys. Res.*, *76*(19), 4381–4401, doi:10.1029/JA076i019p04381.

Baker, D. N., T. I. Pulkkinen, V. Angelopoulos, W. Baumjohann, and R. L. McPherron (1996), Neutral line model of substorms: Past results and present view, *J. Geophys. Res.*, *101*(A6), 12,975–13,010, doi:10.1029/95JA03753.

Blanchard, G. T., L. R. Lyons, J. C. Samson, and F. J. Rich (1995), Locating the polar cap boundary from observations of 6300 Å auroral emission, *J. Geophys. Res.*, *100*(A5), 7855–7862, doi:10.1029/94JA02631.

©2014. American Geophysical Union. All Rights Reserved.

Frey, H. U., S. B. Mende, T. J. Immel, J.-C. Gérard, B. Hubert, S. Habraken, J. Spann, G. R. Gladstone, D. V. Bisikalo, and V. I. Shematovich (2003), Summary of quantitative interpretation of IMAGE far ultraviolet auroral data, *Space Sci. Rev.*, *109*, 255–283.

Jacobs, J. A., S. Matsushita, Y. Kato, and V. A. Troitskaya (1964), Classification of geomagnetic micropulsations, *J. Geophys. Res.*, *69*, 180–181, doi:10.1029/JZ069i001p00180.

Lui, A. T. Y. (1996), Current disruption in the Earth's magnetosphere: Observations and models, *J. Geophys. Res.*, *101*, 13,067–13,088.

Lui, A. T. Y., et al. (2008), Determination of the substorm initiation region from a major conjunction interval of THEMIS satellites, *J. Geophys. Res.*, *113*, A00C04, doi:10.1029/2008JA013424.

Lui, A. T. Y. (2009), Comment on "Tail reconnection triggering substorm onset", *Science*, *324*(5933), 1391, doi:10.1126/science.1167726.

McPherron, R. L. (1970), Growth phase of magnetospheric substorms, *J. Geophys. Res.*, *75*(28), 5592–5599.

Mende, S. B., et al. (2000), Far ultraviolet imaging from the IMAGE spacecraft, *Space Sci. Rev.*, *91*, 287–318.

Mende, S., S. E. Harris, H. U. Frey, V. Angelopoulos, C. T. Russell, E. Donovan, B. Jackel, M. Greffen, and L. M. Peticolas (2008), The THEMIS array of ground-based observatories for the study of auroral substorms, *Space Sci. Rev.*, *141*(1-4), 357–387, doi:10.1007/s11214-008-9380-x.

Mende, S., V. Angelopoulos, H. U. Frey, E. Donovan, B. Jackel, K.-H. Glassmeier, J. P. McFadden, D. Larson, and C. W. Carlson (2009), Timing and location of substorm onsets from THEMIS satellite and ground based observations, *Ann. Geophys.*, *27*, 2813–2830.

Milling, D. K., I. J. Rae, I. R. Mann, K. R. Murphy, A. Kale, C. T. Russell, V. Angelopoulos, and S. Mende (2008), Ionospheric localisation and expansion of long-period Pi1 pulsations at substorm onset, *Geophys. Res. Lett.*, *35*, L17S20, doi:10.1029/2008GL033672.

Murphy, K. R., I. J. Rae, I. R. Mann, D. K. Milling, C. E. J. Watt, L. Ozeke, H. U. Frey, V. Angelopoulos, and C. T. Russell (2009), Wavelet-based ULF wave diagnosis of substorm expansion phase onset, *J. Geophys. Res.*, *114*, A00C16, doi:10.1029/2008JA013548.

Murphy, K. R., I. R. Mann, I. J. Rae, C. L. Waters, B. J. Anderson, D. K. Milling, H. J. Singer, and H. Korth (2012), Reduction in field-aligned currents preceding and local to auroral substorm onset, *Geophys. Res. Lett.*, *39*, L15106, doi:10.1029/2012GL052798.

Nishimura, Y., et al. (2010a), Identifying the driver of pulsating aurora, *Science*, *330*(6000), 81–84, doi:10.1126/science.1193186.

Nishimura, Y., L. Lyons, S. Zou, V. Angelopoulos, and S. Mende (2010b), Substorm triggering by new plasma intrusion: THEMIS all-sky imager observations, *J. Geophys. Res.*, *115*, A07222, doi:10.1029/2009JA015166.

Nishimura, Y., et al. (2010c), Reply to comment by Harald U. Frey on "Substorm triggering by new plasma intrusion: THEMIS all-sky imager observations", *J. Geophys. Res.*, *115*, A12233, doi:10.1029/2010JA016182.

Nose, M., et al. (1998), Automated detection of Pi 2 pulsations using wavelet analysis: 1. Method and an application for substorm monitoring, *Earth Planets Space*, *50*, 773–783.

Pellinen, R. J., and W. J. Heikkila (1978), Observations of auroral fading before breakup, *J. Geophys. Res.*, *83*(A9), 4207–4217, doi:10.1029/JA083iA09p04207.

Rae, I. J., et al. (2009a), Near-Earth initiation of a terrestrial substorm, *J. Geophys. Res.*, *114*, A07220, doi:10.1029/2008JA013771.

Rae, I. J., et al. (2009b), Timing and localization of ionospheric signatures associated with substorm expansion phase onset, *J. Geophys. Res.*, *114*, A00C09, doi:10.1029/2008JA013559.

Rae, I. J., C. E. J. Watt, I. R. Mann, K. R. Murphy, J. C. Samson, K. Kabin, and V. Angelopoulos (2010), Optical characterization of the growth and spatial structure of a substorm onset arc, *J. Geophys. Res.*, *115*, A10222, doi:10.1029/2010JA015376.

Rae, I. J., et al. (2012), The correlation of ULF waves and auroral intensity before, during and after substorm expansion phase onset, *J. Geophys. Res.*, *117*, A08213, doi:10.1029/2012JA017534.

Sakurai, T., and T. Saito (1976), Magnetic pulsation Pi2 and substorm onset, *Planet. Space Sci.*, *24*(6), 573–575.

Samson, J. C., L. R. Lyons, P. T. Newell, F. Creutzberg, and B. Xu (1992), Proton aurora and substorm intensifications, *Geophys. Res. Lett.*, *9*(21), 2167–2170, doi:10.1029/92GL02184.

Sutcliffe, P. R. (1997), Substorm onset identification using neural networks and Pi2 pulsations, *Ann. Geophys.*, *15*, 1257–1264, doi:10.1007/s00585-997-1257-x.

Torr, M. R., et al. (1995), A far ultraviolet imager for the international solar-terrestrial physics mission, *Space Sci. Rev.*, *71*(1–4), 329–383, doi:10.1007/BF00751335.

Voronkov, I. O., E. F. Donovan, and J. C. Samson (2003), Observations of the phases of the substorm, *J. Geophys. Res.*, *108*(A2), 1073, doi:10.1029/2002JA009314.

©2014. American Geophysical Union. All Rights Reserved.